Network model for deep bed filtration

Cite as: Physics of Fluids **13**, 1076 (2001); https://doi.org/10.1063/1.1359747
Submitted: 06 March 2000 . Accepted: 09 February 2001 . Published Online: 12 April 2001

Jysoo Lee, and Joel Koplik

Network model for deep bed filtration

Jysoo Lee[a)]
Department of Physics, Seoul National University, Seoul 151-742, Korea
and Benjamin Levich Institute and Department of Physics, City College of the City University of New York, New York, New York 10031

Joel Koplik
Benjamin Levich Institute and Department of Physics, City College of the City University of New York, New York, New York 10031

(Received 6 March 2000; accepted 9 February 2001)

We study deep bed filtration, where particles suspended in a fluid are trapped while passing through a porous medium, using numerical simulations in various network models for flow in the bed. We first consider cellular automata models, where filtrate particles move in a fixed background flow field, with either no-mixing or complete-mixing rules for motion at a flow junction. The steady-state and time-dependent properties of the trapped particle density and filter efficiency are studied. The complete mixing version displays a phase transition from open to clogged states as a function of the mean particle size, while such a transition is absent in the (more relevant) no-mixing version. The concept of a trapping zone is found to be useful in understanding the time-dependent properties. We next consider a more realistic hydrodynamic network model, where the motion of the fluid and suspended particles is determined from approximate solutions of the time-dependent Stokes equation, so that the pressure field constantly changes with particle movement. We find that the steady-state and time-dependent behavior of the network model is similar to that of the corresponding cellular automata model, but the long computation times necessary for the simulations make a quantitative comparison difficult. Furthermore, the detailed behavior is extremely sensitive to the shape of the pore size distribution, making experimental comparisons subtle. © *2001 American Institute of Physics.* [DOI: 10.1063/1.1359747]

I. INTRODUCTION

Deep bed filtration (DBF) is a common process used to remove solid suspended particles from a fluid.[1–6] A dilute suspension is injected into a filter made of porous material, and the particles are trapped in the interstices or along the walls of the pore space by various mechanisms. Practically speaking, the most relevant properties of this process are the filter efficiency, the fraction of injected particles which are trapped, and the permeability, essentially the inverse of the pressure drop across the filter needed to maintain a constant fluid flux. As more particles are trapped, the filter efficiency and permeability decrease. In practice, after some time the filter is too inefficient or too clogged, and it is then either cleaned or discarded. Theoretically, a number of interesting questions arise as well in DBF. One would wish to predict how the efficiency and permeability of a filter vary with time, in terms of the geometric and other parameters of the system. Obviously, some rather detailed information about the mobility and spatial distribution of the trapped particles is needed, but unfortunately, very little has been available.[7,8]

Recently, Ghidaglia *et al.* carried out a series of well-controlled experiments on deep bed filtration using a random packing of glass spheres as the filter medium.[9–11] In contrast to conventional porous materials such as paper or sandstone, the transparency of glass and the use of an index matched fluid permitted direct visual observation of particle motion inside the filter. In this way, it was possible to determine the density of trapped particles *inside* the filter and monitor the microscopic particle motion, and identify various mechanisms for trapping and subsequent release, in addition to the *external* measurements of the efficiency and permeability.

Such information concerning particle behavior in the interior of a filter has been available only recently, and its understanding is far from complete. For example, consider the density profile of trapped particles, one of the principal quantities describing the inner structure of a filter. At present, we have no firm basis for the prediction of even the likely functional forms of the density, let alone a physical understanding (or predictive ability) starting from the motion of particles at a pore scale. A related question concerns a possible phase transition in steady-state flow in a filter. Neutral non-Brownian particles were used in the experiments by Ghidaglia *et al.*, so that the filtration was a result of geometrical trapping effects. When the radius R of injected particles is small, a small fraction of the particles will be trapped, and the filter efficiency is low, while the filter efficiency will increase as R increases. Based on their experimental data and network simulations, Ghidaglia *et al.* argue that there is a *sharp* transition at a finite value of R, in the limit of infinite system size.[11] They also measured the associated critical exponents, and found them to be near but not

[a)]Present address: Center for Neurodynamics and Department of Physics, Korea University, Seoul 136-701, Korea.

identical, to those of the directed percolation (DP) model.[12] However, the fact that the measurements were not done at steady state, combined with large statistical fluctuations of the data, makes this conclusion open to question.

Network models for transport in porous media are well suited for the study of the behavior of particles and fluid in a filter.[13–16] The pore space of a sphere pack contains relatively large open regions (pores) connected by relatively narrow channels (throats), and is naturally modeled as a ''ball-and-stick'' network. There is a linear relation between pressure drop and fluid flux in each network element, and mass conservation at the nodes provides a set of linear equations for the node pressures, which may be solved numerically.[17] If suspended particles are present, the relationship between the flux and pressure drop relationship is modified but remains linear, and such network models of porous media flow are always mathematically equivalent to a resistor network. Network models are numerically much more tractable than solving the full Stokes equations in the pore space, while retaining enough realism to be compared to experiment.

In this paper, we study two versions of simplified cellular automata (CA) models as well as a hydrodynamic network model, focusing on the evolution of the inner structure of a filter. Cellular automata models have fixed local rules of motion for particle motion on a network and are less realistic than network models, and are therefore not expected to reproduce many of the quantitative details of real filtration. However, due to their simplicity, it is usually possible to obtain a detailed understanding of their behavior by analytic and numerical methods. An analytic solution of a network model is almost impossible to obtain, and its numerical study is severely limited by the large amount of computation time necessary for its simulation. Thus, the study of CA models is complementary to the study of more realistic models for the complete understanding of the filtration process. As will be discussed later, the CA models discussed here share many features that are also valid for the full network model. We feel that the CA model can be used as reference points with which other models can be compared.

Our two versions of the CA model differ in the ''junction rule,'' which specifies the motion of particles across a pore. Particles entering a pore are fully mixed in the ''complete mixing'' version, while such mixing is absent in the ''no-mixing'' version. We study the evolution of the trapped particle density and filter efficiency, and find that their behavior for the two versions is quite different: The steady state of the complete mixing version exhibits a transition from an open state where particles pass through unimpeded (the filter efficiency is 0) to a clogged state where all particles are trapped (the filter efficiency is 1), as the radius of injected particles increases. The transition belongs to the DP universality class.[18] Such a non-trivial transition is absent in the no-mixing version. We find that the trapped particle distribution (or ''trapping zone'' distribution) of a packet is approximately Gaussian. The distribution plays an important role in understanding the time-dependent behavior of the trapped particle density and filter efficiency.

In the network model, we approximate the motion of a particle in a channel by that of a sphere in a cylindrical tube, which can be determined analytically.[19–21] At the flow junctions, a no-mixing rule is used. This rule is adopted based on experimental[10] and numerical[22,23] studies of microscopic motion of non-Brownian particles. Note that the complete mixing is more plausible when diffusion is important, as would be the case for passive and necessarily small tracer particles. We also include the possibility of the ''relaunching'' of a trapped particle by another mobile particle which passes nearby.[10,23] We first consider the case of injecting a single packet of particles. The dependence of penetration depth—the mean distance traveled by the particles before trapping—on the particle radius, the relaunching probability and the packet size is considered. The results from the network model are consistent with experiments. In particular, the ''packet effect'' observed in experiments, an increase of penetration depth with packet size, is reproduced. We next consider the case of particles injected continuously until a steady state is reached. The steady-state filter efficiency increases as the particle radius increases, and the transition region sharpens as the network size increases. We are still very limited in system size (a less than 40×40 network), and we cannot determine with certainty whether there exists a sharp transition in the limit of infinite size. The time-dependent behavior of the steady-state density field and filter efficiency is measured, and is found to be qualitatively similar to that of the CA model.

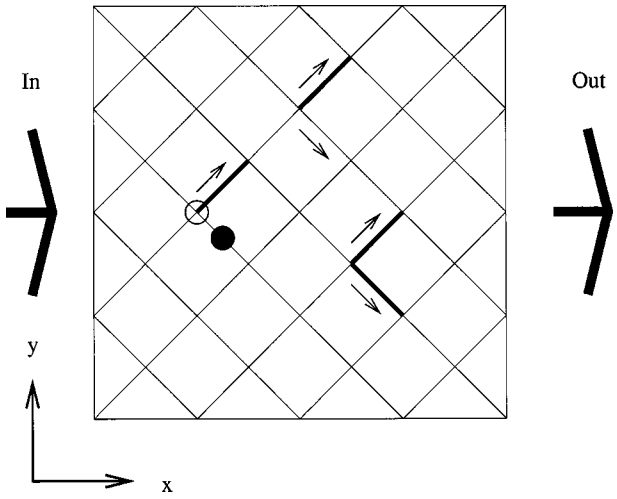

FIG. 1. A schematic view of the model filter: nodes and bonds in a square lattice represent pores and channels in the filter, and *S* and *B* bonds are shown with thin and thick lines, respectively. A moving particle is indicated by an empty circle and a trapped particle with a filled circle. The arrows next to the bonds show the possible movement of a particle. For example, the particle cannot move to the *S* bond with a trapped particle.

II. CELLULAR AUTOMATA MODEL

A. Definition of the model

The cellular automata model is defined on a square lattice, rotated by 45° to the flow axis, of width W and length L, which is an idealized network model of the filter pore space (Fig. 1). The nodes and bonds of the lattice represent pores and channels, respectively. A periodic boundary condition is

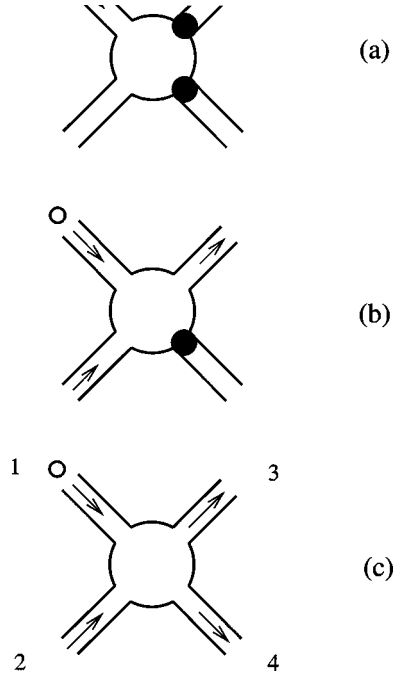

FIG. 2. Different four channel configurations connected to a pore. Particles can move to the right or stay in a channel. Here, we show configurations where (a) two, (b) one, and (c) no exit channels are blocked.

applied in the transverse direction. Fluid containing suspended particles is injected on the left side of the filter ($x=1$ line), and exits the right side ($x=L$ line). Suspended particles, if not trapped, move along the local direction of the fluid flow. We consider particles of radius R, and assign channel radius r_j to bond j, where the radius is drawn from some probability distribution $C(r)$. A bond with $r_j>R$ is called as a B (big) bond, and other bonds ($r_j \leqslant R$) are S (small) bonds. Particles can move through a B bond without difficulty, while they would stick in a S bond. A particle stuck in an S bond ''blocks''—prevents other particles from entering the bond. Let the fraction of S bonds be p. In the model, the fraction is the only relevant quantity from the distribution, and other details of $C(r)$ can be ignored.

The rules for the movement of a particle are as follows. A particle is inserted at a randomly chosen node at the left end and always tries to move to right, the direction of fluid flow. At a node, the particle has to choose one of the two bonds on its right for its motion. If both of the bonds on the right are blocked [Fig. 2(a)], the particle is trapped in the pore, and prevents other particles from entering. In the case that only one of the two bonds is blocked, the particle always moves through the open bond [Fig. 2(b)]. Now consider the case where neither of the two bonds is blocked [Fig. 2(c)]. In ''complete mixing,'' a particle randomly chooses an exit bond with equal probability. The rule is intended to model the situation that diffusion is significant (common for small particles), so particles in a pore are completely mixed. In the ''no mixing'' version, a particle entering a pore by bond 1 (2) always advances to bond 3 (4). This rule is appropriate for the case that the effect of diffusion can be ignored. In such a case (common for nonpassive particles), a particle entering a pore always follows the same trajectory to an exit channel.[10,22,23] Following these rules, the movement of the particle is repeated until either the particle is trapped or comes out of the filter. We then insert another particle to the filter, and the whole process is repeated.

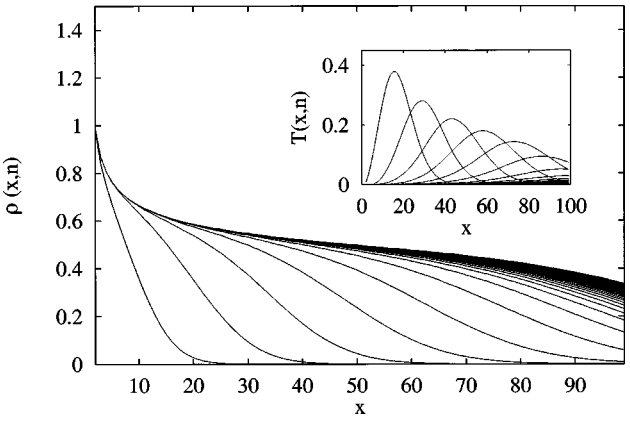

FIG. 3. The density of trapped particles $\rho(x,n)$ for $p=p_c$ after every 500 injections for the cellular automata model with the complete mixing rule. The inset shows the evolution of $T(x,n)$ for the same parameters.

B. Complete mixing

The steady-state behavior of the complete mixing version was studied in Ref. 18, and we give a brief summary of the results here. There is a sharp transition at p_c, which belongs to the directed percolation universality class.[12] The filter efficiency e, the fraction of injected particles that are trapped, changes from 0 (the filter is ''open'') for $p<p_c$ to 1 (''clogged'') for $p>p_c$ in the limit of an infinite system size. We define the density $\rho(x,n)dx$ as the number of trapped particles in $[x,x+dx]$ after injecting n particles into the network. The steady-state density field, $\rho(x)=\lim_{n\to\infty}\rho(x,n)$, was found to have the form $x^{-\beta/\nu_\parallel}F_\pm(x/\xi_\parallel)$. Here, $\xi_\parallel=|p-p_c|^{-\nu_\parallel}$ is the longitudinal correlation length, and $F_\pm(y)$ is a scaling function above/below the transition point. The critical exponents $\nu_\parallel, \beta$ are not known exactly, but accurate numerical estimates are available.[24]

We consider the time-dependent behavior of the density of trapped particles. The particles are injected one by one, so the number of injected particles n can be regarded as a time. We measure $\rho(x,n)$ for several values of p with system size $L=W=100$, and an average is taken over 10^4 samples. In Fig. 3, we show $\rho(x,n)$ for $p=0.3553(\simeq p_c)$ at every 500 injections. For the remainder of this paper, $\rho(x,n)$ is normalized by $2pW$—the average density of S bonds. As n approaches the total number of injected particles (2×10^4), $\rho(x,n)$ saturates to a steady-state curve $\rho(x)$. It is clear that particles are not uniformly trapped. They are mostly trapped near the entrance of the filter for small n, while as n increases, they gradually move farther before getting trapped. The ''trapping zone,'' the region of active trapping, moves downstream through the medium as n increases. The trapping zone can be quantified by plotting the distribution of the locations of trapped particles during δn injections, $T_{\delta n}(x,n)=\rho(x,n)-\rho(x,n-\delta n)$. In the inset of Fig. 3, T at every 500 injections with $\delta n=500$ is shown using the same

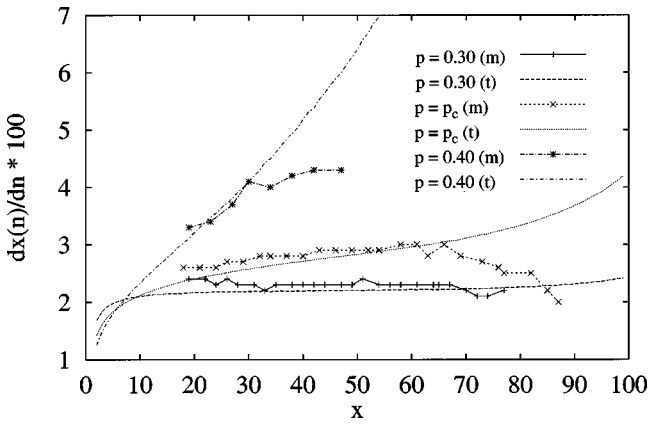

FIG. 4. Velocity of the trapping zone of the cellular automata model with the complete mixing rule versus x for $p=0.3, p_c, 0.4$: measured data, marked with ''m,'' are denoted by symbols, and theoretical curves from Eq. (2)—$1/[2pW\rho(x)]$, marked with ''t,'' are shown by lines.

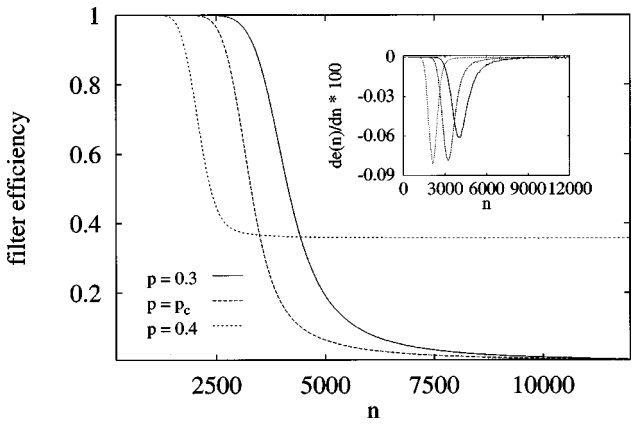

FIG. 5. Time evolution of the filter efficiency for $p=0.3$, 0.3553, 0.4 for the cellular automata model with the complete mixing rule. The inset shows the ''time derivative'' $de(n)/dn$ of the three efficiency curves.

parameters as $\rho(x,n)$. We find that $T(x,n)$ curves are consistent with Gaussian, and can be characterized by the peak position $\overline{x}(n)$, the width of the peak $\delta x(n)$, and the peak value $T_{\max}(n)$. The peak position $\overline{x}(n)$ initially increases with n, and saturates to a p-dependent value. For smaller L, the initial regime of increase is not changed, but the time needed for saturation decreases. The width δx is of order unity for small n, increases and saturates to a value that slowly decreases with p (around 20 at p_c). The saturation time for δx is about the same as that of $\overline{x}$.

The motion of the trapping zone can approximately be related to the steady-state density $\rho(x)$ as follows. For simplicity, we assume that δx is much smaller than the other length scales in the system (e.g., $\overline{x}$). Under this assumption, all the accessible trapping sites are completely filled for $x<\overline{x}(n)$. In other words, $\rho(x,n)=\rho(x)$ for $x<\overline{x}(n)$, and $\rho(x,n)=0$ for larger values of x. If every injected particle is trapped (the filter efficiency is 1),

$$\frac{dn}{2pW}=\int_0^L \rho(x,n+dn)-\rho(x,n)dx$$
$$\simeq\int_{\overline{x}(n)}^{\overline{x}(n+dn)}\rho(x)dx$$
$$\simeq\rho(x)[\overline{x}(n+dn)-\overline{x}(n)]. \quad (1)$$

Thus, the temporal change of $\overline{x}(n)$ is given by

$$\frac{d\overline{x}(n)}{dn}\simeq\frac{\overline{x}(n+dn)-\overline{x}(n)}{dn}\simeq\frac{1}{2pW\rho(x)}. \quad (2)$$

The ''velocity'' of the trapping zone ($d\overline{x}/dn$) as a function of x is plotted for several values of p in Fig. 4. Also shown is the prediction of Eq. (2)—$1/[2pW\rho(x)]$. Overall, the data is in fair agreement with the prediction for small x, but a significant deviation is visible for large x. This observation can be understood by noting that the width of the zone becomes significant for large x, and the filter efficiency decreases from 1 for small x to a p-dependent value for large x. Thus, two of the assumptions used in the derivation of Eq. (2) are valid only for small x.

We next consider the evolution of the filter efficiency $e(n)$. The filter efficiency versus n curves for several values of p are shown in Fig. 5. Here $e(n)$ is close to 1 for small n (all injected particles are trapped), sharply decreases around a p-dependent n, and finally saturates to a p-dependent steady-state value. The shape of the $e(n)$ curve can be understood from the distribution $T(x,n)$ specifying the trapping zone: the efficiency at given n is the fraction of $T(x,n)$ that lies in the medium ($x<L$). For small n, $T(x,n)$ is a rapidly decaying function of x, and its value near the end of the filter ($x=L$) is essentially zero, implying $e(n)$ close to unity. As n increases, the peak position $\overline{x}$ also increases. As $\overline{x}$ approaches L, the fraction of $T(x,n)$ in the medium sharply decreases, and $e(n)$ drops significantly. For larger n, the efficiency slowly approaches to a steady-state value. The value of n where a sharp drop in $e(n)$ is observed is roughly the same n at which $\overline{x}$ reaches L. The transition region can be better shown by taking the ''time derivative'' of the efficiency, $de(n)/dn$, which is the rate of change of $e(n)$ during dn injections. The time derivative $de(n)/dn$ with $dn=100$ using the $e(n)$ curves in Fig. 5 are shown in the inset. We find that the region left to the peak is well described by a Gaussian, but the region right to the peak decays more slowly.

C. No mixing

We begin with the steady-state behavior of the no mixing version of the model. We measure the dependence of the filter efficiency on p for several $L(=W)$ ranging from 10 to 400, averaged over 10^4 samples (Fig. 6). The transition region sharpens as L increases similarly to the complete mixing case, but it seems to move toward the origin. To quantify this motion, we define the ''running'' transition point $p_c(L)$ as the value of p at which the efficiency is $\frac{1}{2}$. In the inset of Fig. 6, $p_c(L)$ is plotted against $1/\sqrt{L}$ (the choice of the x axis will be discussed later). It is clear that $p_c(L)$ becomes very small in the limit of infinite system size, and we argue that

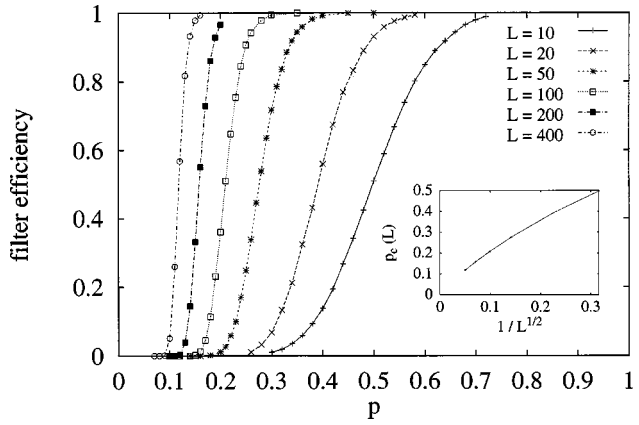

FIG. 6. Dependence of the steady-state filter efficiency on p for several L for the no mixing version of the cellular automata model. The inset shows the dependence of the running transition point $p_c(L)$ on $1/\sqrt{L}$. Here $p_c(L)$ seems to approach 0 as $L\to\infty$.

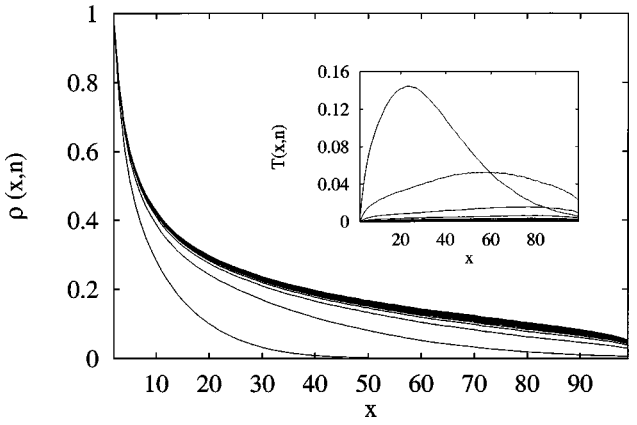

FIG. 7. The density of trapped particles $\rho(x,n)$ of the cellular automata model for $p=0.35$ at every 500 injections. The no mixing rule is used. The inset shows the evolution of $T(x,n)$ for the same parameters.

$p_c(L)$ approaches zero. The absence of a nontrivial transition is in sharp contrast with the case of the complete mixing version. The difference between the two versions of the model can also be seen in the steady-state density of trapped particles $\rho(x)$. We measured $\rho(x)$ for several values of p and L (from 10 to 400), and found it to be exponential at large x, where a faster than exponential decay is observed near the entrance of the filter. Unlike the complete mixing version, no power-law regime is observed.

The main effect of the no mixing rule is the suppression of the transverse motion of the particles, so that their trajectories tend to be straight (except for an alternating zig–zag from column to column, associated with the 45° lattice structure). Consider a particle trajectory around an ''obstacle,'' consisting of blocked S bonds connected together. A mobile particle goes around such an obstacle, and then moves straight through the network. Thus, the ''shadow'' of the obstacle (the region downstream of it) is not accessible to such a particle. The cross-sectional area of the filter that is accessible to the filtrate decreases exponentially with x. In the limit of infinite size, the filtrate cannot reach the end of the filter at any nonzero p, which causes the disappearance of the sharp transition at finite p. In contrast, this shadow region is accessible with the complete mixing rule due to the active transverse motion.

We can make the above argument more quantitative. Assume the trajectories of the particles are straight. To block such a trajectory, one needs two adjacent S bonds, which occurs with probability p^2. Thus, the change in the steady-state density of trapped particles while advancing one lattice site in the x direction is

$$\frac{d}{dx}\rho(x) = -p^2\rho(x), \tag{3}$$

whose solution is

$$\rho(x) = \rho(0)\exp(-p^2x). \tag{4}$$

Using the definition of the running transition point $p_c(L)$,

$$\rho(L)|_{p=p_c(L)} = \rho(0)\exp(-p_c(L)^2L) = \tfrac{1}{2}\rho(0), \tag{5}$$

which implies

$$p_c(L) = \sqrt{\ln 2/L}. \tag{6}$$

Thus, $p_c(L)$ approaches zero as $L\to\infty$, in good agreement with the simulation results (the inset of Fig. 6). The predicted exponential behavior of $\rho(x)$, Eq. (4), is also consistent with the simulations, as previously discussed.

Continuing with the complete mixing version, we consider the time-dependent properties of the density of trapped particles $\rho(x,n)$ and the filter efficiency $e(n)$. In Fig. 7, we show $\rho(x,n)$ at every 500 particle insertions for $p=0.35$ and $L=W=100$. Although the parameters for the figure are similar to those for Fig. 3, $\rho(x,n)$ in the no mixing case decays with x much faster than with the complete mixing rule. This is a consequence of the absence of the transverse motion, which helps particles navigate around the traps. Shown in the inset is the distribution $T(x,n)$, the difference between two successive $\rho(x,n)$ curves. Compared to the complete mixing version, the motion of the trapping zone is much more rapid. We find that Eq. (2), which relates the velocity of the trapping zone with $\rho(x)$ remains valid. Thus, the faster velocity with the no mixing rule is a consequence of the fact that $\rho(x)$ decays faster.

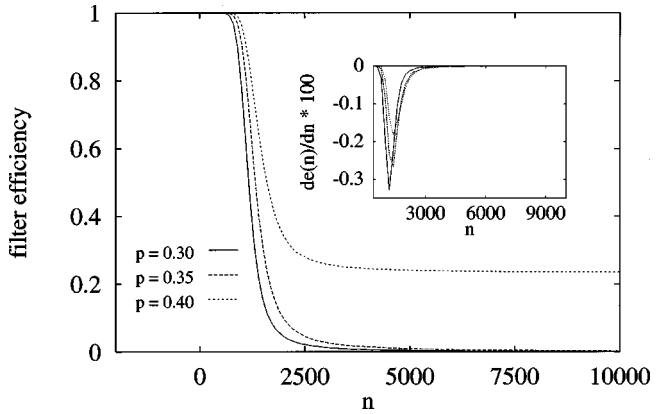

FIG. 8. Time evolution of the filter efficiency of the cellular automata model for $p=0.3$, 0.35, 0.4, using the no mixing rule. The inset shows $de(n)/dn$ of the three efficiency curves.

Last, we discuss the time evolution of the filter efficiency. We show $e(n)$ for several values of p and $L=W=100$ in Fig. 8, and its time derivative $de(n)/dn$ is plotted in the inset. The curves are qualitatively similar to those obtained with the complete mixing rule (Fig. 5). One major difference is that the value of n at which a sharp drop in $e(n)$ is observed becomes much smaller, resulting from the faster motion of the trapping zone.

III. NETWORK MODEL

A. System geometry

In deep bed filtration, the Reynolds number based on the particle size and the local velocity is much smaller than unity (e.g., Ref. 4), and the Stokes equations correctly describe the motion of the fluid. For a given configuration of particles, one can calculate the instantaneous velocity and pressure fields in the fluid, compute the hydrodynamic force exerted on the particles to determine their velocities, and simple time-stepping generates the configuration a short time afterward. By repeating this procedure, one can determine the trajectories of all particles for arbitrary times. In order to make the plan feasible, several simplifications are necessary. The network used in the calculation is the idealized square lattice of the cellular automata model (Fig. 1). Unlike the CA model, the pore radius distribution $C(r)$ must be specified. We choose $C(r)$ to be that of the three-dimensional random close packing (RCP) of uniform spheres, calculated from numerical data for the radial distribution in RCP.[25] The details of the calculation are given in Ref. 18. Since pores are relatively large, the pressure drop across a pore is usually much smaller than that of a channel, and we assume for simplicity that the pressure is constant within a pore. The channels are narrow compared to the pore diameters, and the particles spend a much longer time in them. We assume the particles reside only in the channels if not trapped. Solving the Stokes equation for the whole system is reduced to solving the equation for each channel, which may contains a particle(s), then matching these local solutions.

B. Particles in a channel

For particles in channels, we need a generalization of the Poiseuille formula relating fluid flux to pressure difference, as well as an expression for the velocity of a particle V_p there (which differs from the fluid velocity in general). For simplicity, we assume that the particles are spherical and the throats are cylindrical, and that the particles move only along the center axis of the channels. Approximate solutions for the force and pressure drop on the sphere are available in the limit of small particle radius,[19] using the method of reflections, and in the opposite limit of a tightly fitting sphere, using the lubrication approximation.[10,20] Similar results are also obtained by means of singular perturbation expansions.[21] The results for the latter two cases are not very different, and we use the results of Refs. 20,26.

The pressure drop ΔP across a sphere of radius R in a cylinder of radius r is

$$\Delta P = \frac{12\mu}{\pi r^3} g(\theta) Q, \tag{7}$$

where μ is the fluid viscosity, Q the fluid flux, and $\theta = R/r$. By applying the force-free condition to the sphere, its velocity is

$$V_p = \frac{Q}{\pi R^2} \frac{1}{1-f(\theta)}, \tag{8}$$

where the functions f and g are given by

$$\begin{aligned} f(\theta) &= \frac{(1-\theta)[2(\theta+2)I_2 + (1-\theta)(3\theta+5)I_1]}{6[I_3 + (1-\theta)I_2]}, \\ g(\theta) &= \frac{1}{1-f(\theta)} \left(\frac{\sqrt{2\theta(1-\theta)}}{(1-\theta)^3(1+\theta)} f(\theta) I_3 \right. \\ &\quad \left. - \frac{\sqrt{2\theta(1-\theta)}(\theta+2)}{3(1-\theta)^2(1+\theta)} I_2 \right), \end{aligned} \tag{9}$$

and where the numbers $I_n = \int_{-\infty}^{\infty} dx/(1+x^2)^n$. These equations are obtained for the case $\theta \simeq 1$ (corresponding to tightly fitting particles), and we expect them to become less accurate as θ decreases. In fact, $f(\theta)$ and $g(\theta)$ become negative below a certain value of θ. The actual values of f and g that will be used in the network model are the interpolations between the above expressions and their corresponding values for $\theta = 0$.

If more than one particle is present in a channel, we simply ignore the interaction between the spheres—the relevant limit is the dilute one, and corrections to this approximation are unlikely to be significant (see also Ref. 27). The total pressure drop across the channel is then

$$\Delta P_{\text{channel}} = \frac{8\mu l}{\pi r^4} Q + \frac{4\mu}{\pi r^3} Q[3g(\theta) - 4\theta] n, \tag{10}$$

where l is the length of the channel and n is the total number of spheres in it.

In a typical sphere pack, the length of the channel is comparable to its diameter, so we set $l = 2r$ for the remainder of this paper. When the radius of the particle is larger than that of the cylinder, the particle would stick at the entrance of the throat. In general, the channel would not be completely blocked, but we expect the flux to be greatly reduced.

C. Particles in a pore

At the network level, we must also specify the rules for particle motion *in* a pore. A particle enters a pore from some channel, is carried across it by the flow, and exits through one of several possible downstream channels in general. It is often assumed that the particle flux for a given channel is proportional to the fluid flux there, which is highly plausible in the limit of small particle radius.[28–30] Furthermore, recent studies on the microscopic motion of particles in model porous media show that this approximation is valid even when the radius of the particle is close to that of the channel.[22,23] We thus will adopt this proportionality, also called the flow-induced probability (FIP), henceforth in this paper.

Specifying the flux does not completely determine the motion of the individual particles, and a rule is needed to determine the exit channel for a given entrance channel. A simple and commonly used rule is the complete mixing. One imagines that the particle's Péclet number is sufficiently low that diffusion dominates, and the particle is not confined to its initial streamline and loses all memory of its past history. The particle can then be anywhere in the pore, and chooses its exit channel in proportion to the fluid flux. However, numerical and experimental studies of the microscopic motion of particles in porous media show that the amount of mixing in pores is not extensive, especially for non-Brownian particles.[10,22,23] All particles entering a pore from a particular channel are observed to assume the same trajectory in traversing a pore. In the present network model, we thus use the no mixing rule.

Consider a generic node with four connected channels (Fig. 2). As for the CA model, we suppose that the direction of the motion of the particles is always the same as that of the global flow, so that particles in the two bonds at the left (right) cannot move away from (toward) the node. Deviations from this assumption would only occur when the pore velocity is negligible, a rare occurrence. The rule for the situation that both of the exit channels are blocked [Fig. 2(a)], or that one of them is blocked [Fig. 2(b)] is the same as the CA model. A more interesting situation involves two open exit channels, as shown in Fig. 2(c). Considering the geometry of the pore and the plausible trajectories within it, a particle entering channel 1 (2) will tend to proceed to channel 3 (4), and we impose the following flux-based rule for particles entering channel 1. Denoting the fluid flux through channel i as q_i, if $q_1 \leqslant q_3$, the particle always exits through channel 3. If $q_1 > q_3$, we pick a random number h in the interval [0,1]. If $q_1 h \leqslant q_3$, the particle proceeds to channel 3; otherwise the particle exits through channel 4. The rule for a particle enters through channel 2 and is similarly defined with appropriate changes of the indices. The randomness is due to our lack of knowledge of the displacement of the particle from the center axis of its incoming cylinder, and the rule is based on a picture of particle trajectories not crossing in the pores.

The particles can also interact with each other. The actual form of the interaction between two suspended particles can be very complex,[23] and it is difficult to obtain general rules. In this paper, we neglect interaction effects on the local velocity and pressure fields, but we do consider the ''relaunching'' of geometrically trapped particles. It is observed experimentally that for a mobile particle passing near a trapped one can allow the latter to escape (or be ''relaunched'') from the trap.[10] Such relaunching effects are also found in Stokesian dynamics simulations of particles motion through model porous media.[23] The reason for specifically including relaunching is that it may change the distribution of the trapped particles, and the temporal behavior of the filter. Unfortunately, no quantitative measurements or calculations that give conditions for relaunching are available. Following Ref. 10, we introduce the relaunching probability γ, which is the probability that a trapped particle escapes when another mobile particle is present in the same pore.

D. Simulation algorithm

We now combine the above rules of motion to construct a network model of particulate motion. The configuration at a given time is characterized by the locations of the particles, which can only reside in the channels. Particles can reside at any location along the center axis of the channels. Since the pressure–flow relation for a channel is linear, as given in Eq. (10), the determination of the pressure field becomes that of solving the discretized Laplace equation. Since the configuration changes gradually over time, an iterative procedure is natural, and we employ the conjugate-gradient method.[31] As a convergence criterion, we use the condition that the difference of the average pressures between two successive iterations is smaller than 10^{-5}.

If a channel with a trapped particle is assumed to carry zero fluid flux, for large number of trapped particles a portion of the network can be nearly isolated from the rest. In such situations, the pressure field in the detached portion of the network converges very slowly, which slows down the convergence of the entire network. If we assign a small but finite permeability to such bonds (typically 0.01% of the open channel value), the convergence is more rapid while there is essentially no probability for a particle to enter such a bond. Assigning small but nonzero flux is also physically reasonable, as described previously.

Having determined the pressure field, we calculate the velocity of the particles from Eq. (8). If the particles remain in their current channel, the network equations are unchanged, so an update is needed only when a particle reaches a pore. For each particle, we thus calculate the time τ needed to reach the end of the channel, and construct an event calendar[32] by collecting and sorting the values of τ for all the particles. We choose the smallest τ from the calendar, and advance the time of the system by that amount. The particle that corresponds to the chosen τ will reach the end of the channel, and proceeds to another channel given by the rules described in the previous section. Other particles advance along the channels they currently occupy, by an amount given by the velocity of the particle. We then solve for the pressure field for the new configuration, and update the event calendar. This procedure is repeated to calculate the time evolution of the particle distribution.

E. Single packet injection

We begin a simulation with a fresh filter, containing pure fluid. A packet of particles is inserted at random locations along the $x=1$ line (Fig. 1), moves through the network, and eventually either is trapped or exits the network. We then insert another packet, and again wait for it to be either trapped or exit. In this section, we consider the case that only single packet of n_p particles is injected. The idea is to study first a simpler situation in the absence of interpacket interaction, which is always present in general. We focus on the penetration depth λ, which is the average downstream (x) distance traveled by the particles before being trapped.

Consider first the very simple case of $n_p=1$. We measure λ for several p with $L=100$ and $W=50$, where the average is taken over 10^3 particles (Fig. 9). Since p is the

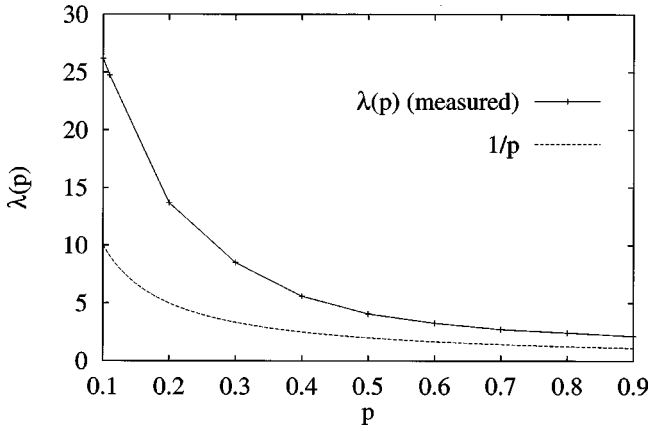

FIG. 9. The penetration depth $\lambda(p)$ of the network model as a function of p for single-particle injection, for system size $L=100$ and $W=50$. Also shown is $1/p$, the penetration depth without FIP.

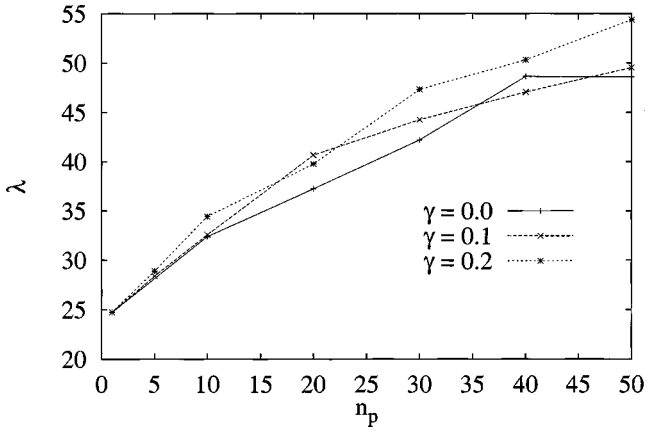

FIG. 10. The penetration depth λ of the network model versus n_p with $\gamma=0, 0.1, 0.2$ for single packet injection, for system size $L=100$, and $W=50$. The curve is an average over about 5000 samples.

fraction of S bonds that serve as trapping sites, the penetration depth in the absence of FIP is $1/p$. As shown in the figure, the measured λ is always larger than $1/p$. The reason for the difference is that FIP helps the particles to avoid traps by reducing the probability for the particle to choose S bonds whose fluid flux is small.

Comparing λ from the simulations with the experiments for a random close packing,[10] we find that the shape of $\lambda(p)$ curve is very similar, but the numerical values are quite different. For example, the value of λ at $\theta=R/r=0.162$ ($p \simeq 0.11$ for RCP) from the simulations is 24.7, much larger than the experimental value of 8.4. Note that R is the radius of the injected particle, and r is that of the particles of the packing. The values from the simulations are always larger than those from the experiments. The network used in the simulations is two dimensional, and its topology is different from that of RCP, so some discrepancies are to be expected, but not the gross differences observed.

A possible explanation for the discrepancy is the following. In the experiments, the maximum radius of an injected particle without trapping is 0.140,[10] which is distinctly smaller than the geometrical minimum channel radius, $2/\sqrt{3}-1 \simeq 0.1547$. (Here the radii are normalized by the radius of the particles making up the sphere pack.) The fact that particles do not pass through a channel even though their radius is smaller than the nominal channel size might be rationalized in terms of surface roughness, or the effects of nonhydrodynamic interactions, and it is even sufficient to suppose that the transit time of a particle becomes large when its radius is comparable to that of the channel. In this situation, the ''effective'' radius of a particle is larger than its physical radius, and a reasonable estimate of the magnitude is given by the experimental difference $\simeq 0.015$. The penetration depth λ using the effective radius is much closer to the experimental value: for example, λ for $\theta=0.162$ is 13.7, instead of 24.7. After taking into account the $\sqrt{2}$ factor of the square lattice, the λ from the simulations is 9.7, compared to the experimental value of 8.4. The agreement is similar for other values of θ.

The values of λ from the present simulations are larger, by about a factor of 3 for $\theta=0.162$, than those of the network simulations of Ghidaglia *et al.*[10] The network model used in their simulations is different from the present one in the channel radius distribution $C(r)$ as well as a few minor points (e.g., the flow–pressure relation is slightly different). The distribution $C(r)$ used in Ref. 10 is $(r-r_g)^{-1/2}$ with the interval of $[r_g, r_g+\frac{1}{4}]$, where r_g is the minimum channel radius $2/\sqrt{3}-1$. Again, r and r_g are normalized by the radius of the particles of the packing. We repeat the simulations of the present network model using the power law distribution with no other change, and find that the values of λ become comparable to those of their simulations.

We next consider the case of $n_p>1$. Besides p, two additional parameters affect λ: n_p itself and the relaunching probability γ. First, p is fixed at 0.11 (or $\theta=0.162$), and n_p and γ are varied. In Fig. 10, the dependence of λ on n_p is plotted for $\gamma=0$,0.1 and 0.2. Here, $L=100$ and $W=50$, and λ is averaged over about 5000 particles. Here λ increases monotonically with n_p, a behavior similar to the that in the experiments of Ghidaglia *et al.*[10] The value of λ at $n_p=50$ is about twice the value at $n_p=1$, and the relative increase is comparable to the experimental value. It also can be seen in the figure that λ has little systematic dependence on γ. To check this dependence, λ is measured with γ up to 0.5 and $n_p=5$, 10, 20. We find that λ is an increasing function of γ, but the rate of increase is small. λ for $\gamma=0.5$ is about 15% larger than that for $\gamma=0$. A very rough estimate of γ, based on Stokesian dynamics simulations on model porous media, is a few percent (less than 0.1).[23] We thus expect that the effect of relaunching is not very significant. For the remainder of this paper, γ is fixed to 0.1.

One may wonder how a packet of particles travels farther than a single particle without relaunching. Consider a packet of particles passing a trapping site. If one of the particles is trapped, it prevents other particles from being trapped, so the other particles in the packet bypass the site, resulting in increased λ. The dependence of λ on n_p in the absence of relaunching is less strong in the network model of Ghidaglia *et al.*[10] The complete mixing rule was used in the model, and transverse spreading of a packet is significant (of

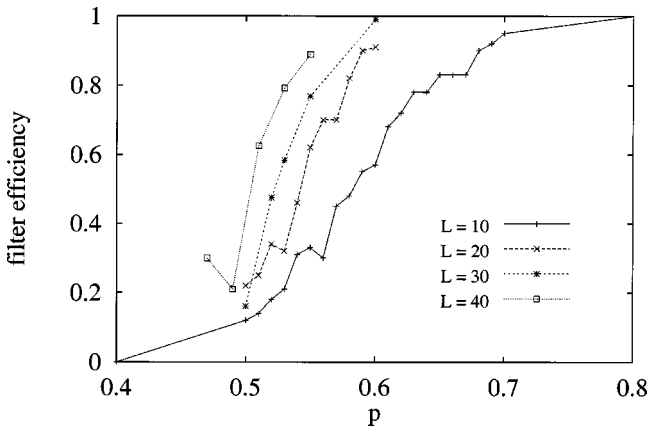

FIG. 11. The steady-state filter efficiency versus p for the network model. Particles are injected one by one until a steady state is reached. The number of samples in the average ranges from 100 ($L=10$) to 40 ($L=40$).

order $\sqrt{x}$). Due to the spreading, the interaction between the particles in a packet decreases, which may explain the weak dependence on n_p. On the other hand, transverse spreading is rather small (about two lattice units) in the present simulations. The results from the simulations for other values of p (0.2 and 0.3) are essentially the same.

F. Continuous injection: Steady-state behavior

We now consider the more interesting case of sequentially injecting packets of n_p particles. Only the case of $n_p=1$ will be considered, and in this section, the steady-state behavior of the model will be discussed. We assume that a steady state is reached if 100 consecutive injected particles exit the filter (the filer is open), or 100 consecutive attempts to inject a new particle fail (the filter is clogged). The no mixing rule used in the network model suggest that the model is similar in its behavior to the no mixing version of the CA model. However, the dynamics of the particles for the network model is given in terms of the global pressure field, compared to the local dynamics used in the CA model. And, it is quite possible that the network model behaves differently from the version of the CA model.

The simulations are done on square networks of sizes $L=10$, 20, 30, and 40. For each L, from 27 ($L=10$) to 5 ($L=40$) different values of p are studied. The number of samples for given L and p varies from 100 ($L=10$) to 40 ($L=40$). The steady-state filter efficiency versus p is shown in Fig. 11. The transition region sharpens as L increases, and the running transition point $p_c(L)$ decreases with L. However, a limited system size as well as significant noise makes the prediction of the behavior in the $L\to\infty$ limit difficult: the present data is compatible with both zero and nonzero p_c in this limit. Studies of large systems with more samples are clearly necessary, but the required computation time becomes too large. The simulations of 10 samples of the $L=20$ system typically takes about 1 CPU hours on a single node of Cray T3E (450 MHz Alpha 21164 processor), but takes 10 and 25 CPU hours for $L=30$ and 40, respectively. It is probably necessary to study 1000 samples of the $L=100$ system at each p for a definite answer, and that is beyond the limit of our computational capability.

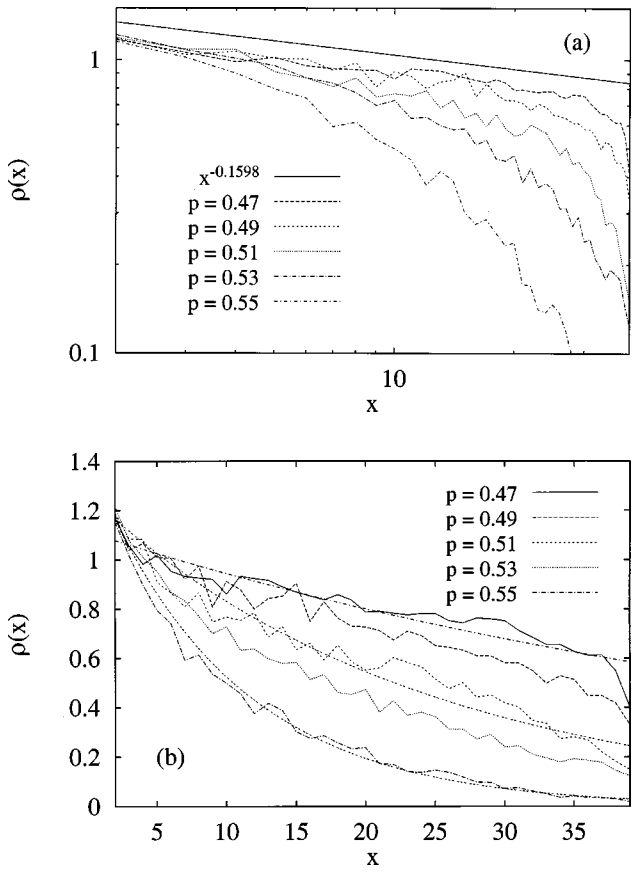

FIG. 12. The steady-state density of trapped particles of the network model for several p, in a square network with $L=40$. Particles are injected one by one until a steady state is reached. In (a), the data are shown on a log–log plot to test for a DP class transition. Also shown is power law curve $x^{-\beta/\nu_\parallel}$ with DP exponents. In (b), the same data are plotted using a linear scale, along with exponential fits for $p=0.47$, 0.51, 0.55.

We next consider the steady-state density of trapped particles. A log–log plot of $\rho(x)$ for several p around the running critical point $p_c(L)$, for $L=40$ is shown in Fig. 12(a). If there exists a transition in the DP universality class, $\rho(x)$ at the transition point would be given by $x^{-\beta/\nu_\parallel}$ (also shown in the figure), where $\beta/\nu_\parallel$ is approximately 0.1598.[24] The simulation data for $p=0.49$ are well described by a power law with the DP exponent, and $\rho(x)$ for other values of p is consistent with a DP transition, which is confirmed by fair quality of ''data collapse'' using DP exponents. However, the range over which $\rho(x)$ can be fitted by a power law is very limited (less than one decade), and the range of p studied is too narrow. Furthermore, the measured $\rho(x)$ is also consistent with an exponential behavior. In Fig. 12(b), the same $\rho(x)$ data are shown in a linear scale, plotted along with the exponential fit for the $p=0.47$, 0.51, and 0.55 data. The decay constant from the fit for a given p seems to converge as L increases, and the convergent value is consistent with the p^2 form in Eq. (4). Again, the asymptotic behavior of $\rho(x)$ is not apparent in the small systems considered here, and a study of larger systems is clearly necessary. We also checked the effect of the relaunching probability on the

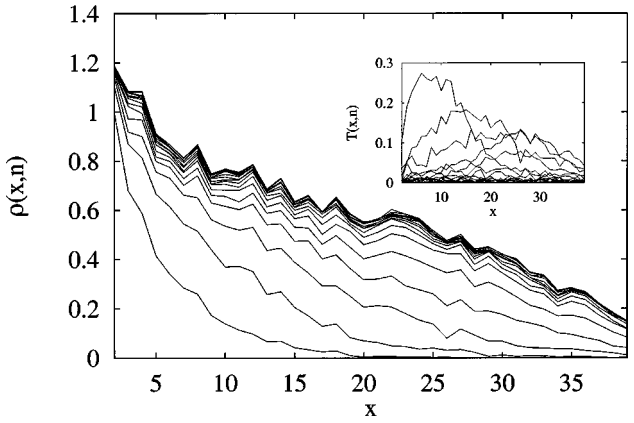

FIG. 13. The density of trapped particles $\rho(x,n)$ for $p=0.51$ after every 200 injections for the network model, in a square network with $L=40$. The inset shows the evolution of $T(x,n)$ for the same parameters.

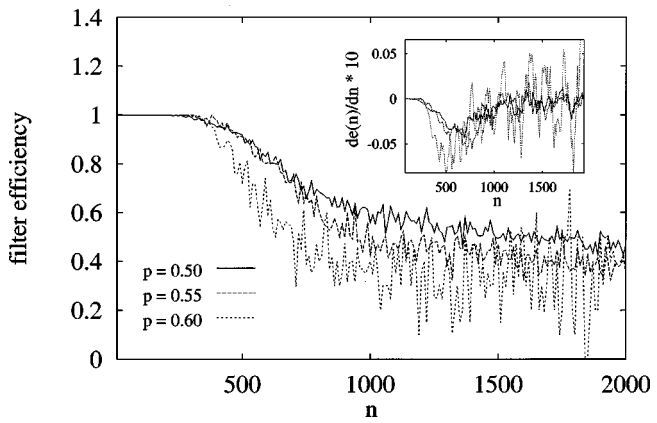

FIG. 15. Time evolution of the filter efficiency of the network model for $p=0.50$, 0.55, 0.60, in a square network with $L=30$. The inset shows $de(n)/dn$ for the three efficiency curves.

steady-state density, by measuring $\rho(x)$ for three values of γ (0,0.05,0.1) for each of three values of $p=0.5$, 0.55, 0.6, where L is fixed to 20. At each p different values of γ produce density profiles that fluctuate weakly about each other, but no systematic dependence was observed.

G. Continuous injection: Time-dependent behavior

Last, we discuss the time evolution of the density of trapped particles $\rho(x,n)$. In Fig. 13, we show $\rho(x,n)$ at every 200 injections for $L=40$ and $p=0.51$. Here $\rho(x,n)$ saturates to a steady-state curve $\rho(x)$ at $n\sim10^3$. Similarly to the CA model, the particles are not uniformly trapped, and the trapping zone moves down as n increases. The qualitative behavior of $\rho(x,n)$ is similar to that of the CA model (Figs. 3 and 7). For a better comparison, we show the distribution $T(x,n)$, the difference between the two successive $\rho(x,n)$ curves, in the inset. The distribution $T(x,n)$, although noisy, can again be fit with a Gaussian, parametrized by the peak position $\overline{x}(n)$, the width of the peak $\delta x(n)$, and the peak value $T_{\max}(n)$. We find that $\overline{x}(n)$ increases with n and saturates to a value that depends weakly on p. The saturation time is about the same as that for $\rho(x,n)$. Following the study of the CA model, we consider the velocity $d\overline{x}(n)/dn$ as a function of x. The velocity for several p at $L=40$ is shown in Fig. 14. Also plotted is the theoretical velocity given in Eq. (2), obtained by relating it to $\rho(x)$. Although the measured data are very noisy, it seems to be consistent with the theory. Due to large fluctuations, a quantitative comparison of the time-dependent quantities (e.g., $\overline{x}$) with those of the CA model is not possible.

We then consider the evolution of the filter efficiency $e(n)$. In Fig. 15, the filter efficiency versus n for several p with $L=30$ are shown. Here $e(n)$ is close to 1 for small n, and starts to decrease around a p-dependent n. It seems to saturate at large n, but large fluctuations present make the behavior uncertain. Also shown in the inset is the time derivative $de(n)/dn$ of the $e(n)$ curves. The curve is qualitatively similar to that of the CA model (Figs. 5 and 8). The time evolution of the permeability of the filter is an important quantity in practice, and we have determined it as well. The permeability of the filter in the network model, normalized to that of the fresh filter, is plotted against n in Fig. 16. The permeability initially decreases exponentially, then the rate of decrease becomes smaller. Such a ''two-step'' process is commonly observed for other values of p and L.

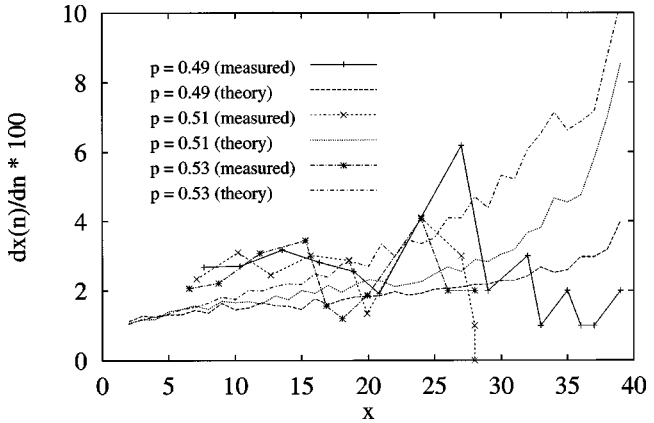

FIG. 14. The velocity of the trapping zone of the network model versus x for $p=0.49$, 0.51, 0.53: measured points are indicated by symbols, and theoretical curves from Eq. (2)—$1/[2pW\rho(x)]$ are shown by lines.

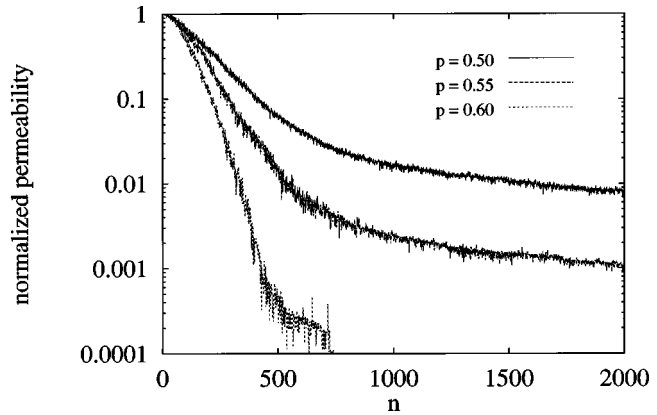

FIG. 16. Time evolution of the permeability of filter of the network model for $p=0.50$,0.55,0.60, in a square network with $L=30$. The permeability is normalized to that of a fresh filter.

IV. SUMMARY

We have studied simple cellular automata models and a more elaborate network model for deep bed filtration. The CA models, which assume a fixed background flow in which the filtrate particles move, are computationally simple enough to study their behavior at large scales and to reliably examine scaling and other behavior. It is found that two versions of the CA model, differing in the junction rule, behave very differently. The steady state of the complete mixing version exhibits a transition in the DP universality class from open to clogged states. This nontrivial transition is absent in the no mixing version, which is more relevant to the DBF process. The CA results motivate consideration of the spatial distribution of the trapping zone, $T(x,n)$, which is found to be very useful in understanding the evolution of quantities such as the filter efficiency and the density of trapped particles.

We then turned to a more realistic dynamic network simulation, based on approximate local solutions of the Stokes equations. Here we find that the results from packet injection are consistent with previous experiments and the corresponding CA model. However, the quantitative behavior is very sensitive to the details of the pore size distribution, and quantitative agreement in calculations of this type may be absent or fortuitous. In the case of continuous injection, no experimental comparison is available, but the filter efficiency and the trapped particle density are qualitatively similar to those of the CA model. However, the calculations are computationally expensive and not practicable for networks of size greater that 40×40 or so. As a result, we have a limited range of system sizes, and large statistical fluctuations as well, making a quantitative comparison and analysis of scaling behavior difficult.

The question of a phase transition between open and clogged filter states is a particularly interesting one, since it would be very desirable to place this problem in the context of a universality class with known properties. Unfortunately the computational demands of the required analysis are too great: as in analogous problems in dense suspensions, the presence of a mobile flow geometry with microscopic variations limits any realistic simulation to modest sizes. A further difficulty is that of the spatial dimension—although some three-dimensional properties such as permeability can be recovered by a judiciously chosen two-dimensional model, phase transitions are very sensitive to dimension. Our network methods are easy to formulate in three dimensions, but the system size limitations would be more severe. New approaches to the problem seem to be required.

ACKNOWLEDGMENTS

We thank E. Guazzelli, L. de Arcangelis, and S. Redner for stimulating discussions. This work is supported by the Geosciences Research Program, Office of Basic Energy Sciences, U.S. Department of Energy. One of us (J.L.) is supported in part by SNU-CTP and the Korea Science and Engineering Foundation through the Brain-Pool program. The simulations were performed on the Cray T3E at the Korea Research and Development Information Center.

[1] J. Herzig, D. Leclerc, and P. LeGoff, ''Flow of suspensions through porous media: Application to deep bed filtration,'' Ind. Eng. Chem. **62**, 8 (1970).
[2] S. Goren, ''Matrix Filtration, a Tutorial,'' in *Physical Separations*, edited by M. Freeman and J. FitzPatrick (Engineering Foundation, New York, 1977), pp. 535–548.
[3] J. Dodds, G. Baluais, and D. Leclerc, ''Filtration process,'' in *Disorder and Mixing*, edited by E. Guyon, J. Nadal, and Y. Pomeau (Kluwer, Dordrecht, 1988), pp. 163–183.
[4] C. Tien, *Granular Filtration of Aerosols and Hydrosols* (Butterworths, Boston, 1989).
[5] S. Datta and S. Redner, ''Gradient clogging in depth filtration,'' Phys. Rev. E **58**, R1203 (1998); ''Gradient and percolative clogging in depth filtration,'' Int. J. Mod. Phys. C **9**, 1535 (1998).
[6] S. Redner and S. Datta, ''Clogging time of a filter,'' Phys. Rev. Lett. **84**, 6018 (2000).
[7] O. Lamrous, D. Houi, C. Zarcone, and J. Pradere, ''Magnetic resonance imaging application to study porous media,'' Rev. Phys. Appl. **24**, 607 (1989).
[8] D. Houi, ''Filtration and porous media,'' in *Hydrodynamics of Dispersed Media*, edited by J. Hulin, A. Cazabat, and E. Carmona (Elsevier, Dordrecht, 1990), pp. 155–173.
[9] C. Ghidaglia, E. Guazzelli, and L. Oger, ''Particle penetration depth distribution in deep bed filtration,'' J. Phys. D **24**, 2111 (1991).
[10] C. Ghidaglia, L. de Arcangelis, J. Hinch, and E. Guazzelli, ''Hydrodynamic interactions in deep bed filtration,'' Phys. Fluids **8**, 6 (1996).
[11] C. Ghidaglia, L. de Arcangelis, J. Hinch, and E. Guazzelli, ''Transition in particle capture in deep bed filtration,'' Phys. Rev. E **53**, R3028 (1996).
[12] A. Aharony and D. Stauffer, *Introduction to Percolation Theory* (Taylor and Francis, London, 1992).
[13] M. Leitzelement, P. Maj, J. Dodds, and J. Greffe, ''Deep bed filtration in a network of random tubes,'' in *Solid Liquid Separation*, edited by J. Gregory (Ellis, Harwood, 1984), pp. 273–296.
[14] S. Rege and H. Fogler, ''A network model for deep bed filtration of solid particles and emulsion drops,'' AIChE J. **34**, 1761 (1988).
[15] M. Sahimi and A. Imdakm, ''Hydrodynamics of particulate motion in porous media,'' Phys. Rev. Lett. **66**, 1169 (1991).
[16] J. Hampton, S. Savage, and R. Drew, ''Computer modeling of filter pressing and clogging in a random tube network,'' Chem. Eng. Sci. **48**, 1601 (1993).
[17] J. Koplik, ''Creeping flow in two-dimensional networks,'' J. Fluid Mech. **119**, 219 (1982).
[18] J. Lee and J. Koplik, ''Simple model for deep bed filtration,'' Phys. Rev. E **54**, 4011 (1996).
[19] See, e.g., J. Happel and H. Brenner, *Low Reynolds Number Hydrodynamics* (Nijhoff, The Hague, 1983).
[20] N. Özkaya, Ph.D. thesis, Columbia University, 1985.
[21] P. Bungay and H. Brenner, ''The motion of a closely fitting sphere through a fluid-filled tube,'' Int. J. Multiphase Flow **1**, 25 (1973).
[22] D. Audet and W. Olbricht, ''The motion of model cells at capillary bifurcations,'' Microvasc. Res. **33**, 377 (1987).
[23] J. Lee and J. Koplik, ''Microscopic motion of particles flowing through a porous medium,'' Phys. Fluids **11**, 76 (1999).
[24] For example, J. Essam, A. Guttmann, and K. Da'Bell, ''On two-dimensional directed percolation,'' J. Phys. A **21**, 3815 (1988).
[25] G. Mason, ''Radial distribution function for small packings of spheres,'' Nature (London) **217**, 733 (1968).
[26] There are small differences between the results presented here and those of Ref. 20, which originate from different ways of handling nonsingular contributions. The quantities of interest agree with each other to within 1%.
[27] R. Ditchfield and W. L. Olbricht, ''Effects of particle concentration on the partitioning of suspensions at small divergent bifurcations,'' J. Biomech. Eng. **118**, 287 (1996).
[28] P. G. Saffman, ''A theory of dispersion in a porous medium,'' J. Fluid Mech. **6**, 321 (1959).
[29] M. Sahimi, H. Davis, and L. Scriven, ''Dispersion in disordered porous media,'' Chem. Eng. Commun. **23**, 329 (1983).
[30] S. Rege and H. Fogler, ''Network model for straining dominated particle entrapment in porous media,'' Chem. Eng. Sci. **42**, 1553 (1987).
[31] W. Press, S. Teukolsky, W. Vettering, and B. Flannery, *Numerical Recipes* (Cambridge University Press, Cambridge, 1992).
[32] See, e.g., D. C. Rapaport, *The Art of Molecular Dynamics Simulation* (Cambridge University Press, Cambridge, 1995).